Chempublish Journal
Journal Homepage: online-journal.unja.ac.id/chp
Department of Chemistry
Faculty of Science and Technology
Universitas Jambi
ISSN (Online): ISSN 2503-4588
No. 23/E/KPT/2019

Article

Impact of magnetite on Fe_3O_4/Activated Carbon (AC)/ZnO Nanocomposite for Photodegradation of Rhodamine B

Restina Bemis[1*], Lenny Marlinda[1], Rahmi[1], Nurul Pratiwi[1], Putu Adityo Wibimanyu[1], Lia Anggresani[2,3]

[1]Department of Chemistry, Faculty of Science and Technology, Universitas Jambi, Indonesia
[2]Graduate School of Engineering, Gifu University, Yanagido 1-1, Gifu-Shi, Gifu, Japan
[3]Department of Midwifery, Syedza Saintika University, Padang City, West Sumatera, Indonesia

Abstract

Rhodamine B is an organic dye commonly used in the textile industry, but it is toxic. Therefore, a photodegradation method using Fe_3O_4/activated carbon (AC)/ZnO nanocomposite is necessary to address environmental issues caused by rhodamine B. The Fe_3O_4/AC/ZnO nanocomposite has been successfully synthesized using the sonication method. Iron sand is used as a source of magnetite (Fe_3O_4), coconut shells as a source of activated carbon, and Zinc nitrate as a source of ZnO. XRF results show that the Fe content in iron sand is 74.10%. The ratio of Fe_3O_4 addition used in Fe_3O_4/AC/ZnO nanocomposite is 0:1:1; 1:1:1; 2:1:1; 3:1:1; 4:1:1. XRD characterization shows that the 1:1:1 ratio of Fe_3O_4/AC/ZnO nanocomposite has the smallest crystal size of 48.17 nm. The addition ratio of Fe_3O_4 does not affect the structure of the formed Fe_3O_4/AC/ZnO nanocomposite. Fe_3O_4/AC/ZnO nanocomposite is formed at 2theta 30.23°; 35.60°; 57.11°; and 62.83° for Fe_3O_4, peak broadening at 26.72° and ~44.71 for AC, and 31.82°; 34.47°; 36.30°; 47.59°; 56.63°; 62.89° and 67.98° for ZnO. SEM results show particle sizes of 57.95 nm for ZnO and 42.74 nm for Fe_3O_4/AC/ZnO 1:1:1 nanocomposite. VSM showed saturation magnetism of 4.41 emu/g for Fe_3O_4/AC/ZnO 1:1:1 nanocomposite and 28.8 emu/g for Fe3O4. The photocatalytic test showed that the Fe_3O_4/AC/ZnO 1:1:1 nanocomposite had the best % degradation of rhodamine B, at 96.1%, under sunlight.

Keywords: *Magnetite: nanocomposite Fe3O4/AC/ZnO; photodegradation; rhodamine B.*

* Corresponding author
Email addresses: restina@unja.ac.id

DOI: https://doi.org/10.22437/chp.v9i2.47812
Received August 14th 2025; **Accepted** November 11th 2025; **Available online** December 25th 2025

Graphical Abstract

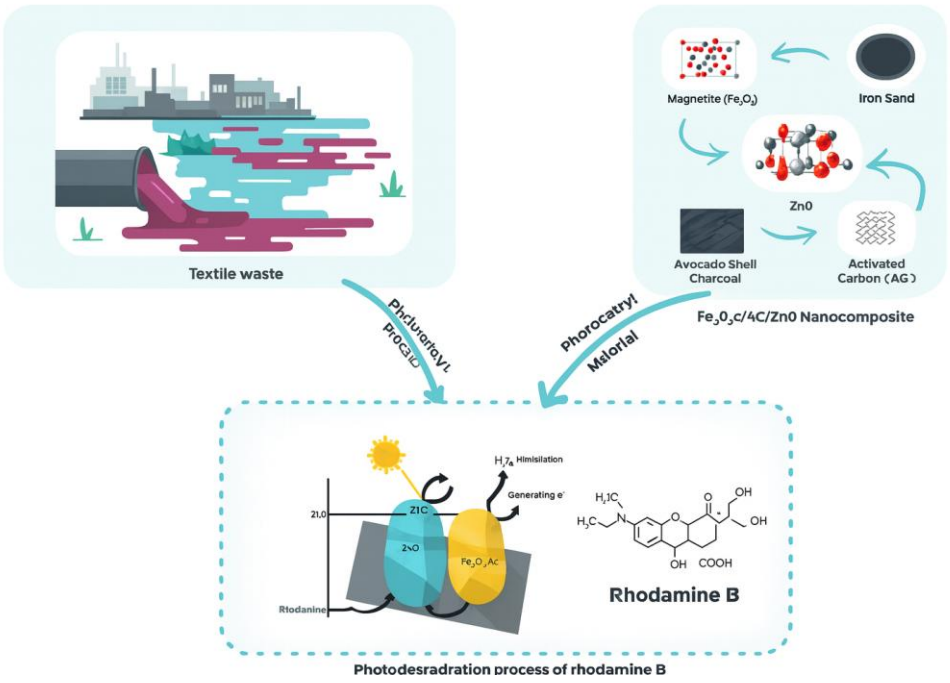

Introduction

Rhodamine B ($C_{28}H_{31}ClN_2O_3$) is a synthetic xanthene dye widely utilized in the textile industry due to its low cost, high color intensity, and ease of availability. However, rhodamine B poses serious health risks, as exposure through skin contact, eye contact, or ingestion can lead to toxic effects, including irritation, organ damage, and potential carcinogenicity [1]. In addition to its adverse health impacts, rhodamine B is environmentally persistent and can contaminate aquatic ecosystems if discharged untreated. Therefore, effective treatment of textile wastewater containing rhodamine B is essential prior to its release into the environment.

Various physical and chemical treatment methods have been investigated to address dye-containing wastewater, such as photolysis [2], electrocoagulation [3], and photo-Fenton oxidation processes [4]. Although these techniques are capable of achieving high removal efficiencies, their practical application is often limited by several drawbacks. These include high chemical consumption, substantial electrical energy requirements, operational complexity, elevated maintenance costs, and the generation of secondary pollutants such as sludge that require further handling and disposal [5]. Consequently, there is a growing need to develop alternative treatment approaches that are not only effective but also economically feasible and environmentally sustainable.

Photodegradation is one of the most widely chosen technologies today. The photodegradation method is based on photocatalysts derived from semiconductor materials because they are arranged and have a very high potential space dimension. In photocatalyzed oxidation, UV light provides energy that can be used to produce electron-hole pairs. Electron-hole pairs will diffuse to the surface of oxide particles that oxidize pollutants [6]. In general,

photocatalysts are often used. ZnO is a material that has a broad band gap energy (Eg) of 3.37 eV and a binding energy of 60 MeV, so it has great potential to be used as a photocatalyst [7].

ZnO in photodegradation still has some shortcomings, so modification of the ZnO surface is needed. Usually, modification is done with activated carbon, which acts as a surface area giver on ZnO, but in ZnO / activated carbon photocatalysts, it is still difficult to remove or recover photocatalysts that have been used, which can cause secondary pollution [8]. Therefore, Fe_3O_4 was added as a contributor to magnetic properties. This addition facilitates separation after the photocatalysis process and increases the photocatalytic activity of Fe_3O_4/AC/ZnO nanocomposites. Fe_3O_4 has magnetic properties with a gap energy of 2.69 eV [9]. It also has a large surface area, good biocompatibility, low toxicity, and efficient light absorption in the visible light region [10]. Fe_3O_4 can optimize the separation of electron (e-) and hole (h+) pairs. It does so by facilitating the transfer of excited electrons from the valence band to the conduction band. Furthermore, the excellent magnetic properties of Fe_3O_4 will facilitate the separation of photocatalyst materials from their solutions using an external magnetic field [11]. Research conducted by Wang (2021) showed an increase in Rhodamine B photodegradation efficiency, from 71.13% with ZnO to 76.46% with Fe_3O_4/ZnO, with band gap and saturation magnetization (Ms) values of 2.86 eV and 44.77 emu/g for Fe_3O_4/ZnO [12]. In this study, Fe_3O_4/AC-ZnO was synthesized by varying the ratio of Fe_3O_4 addition to AC/ZnO. The aim was to analyze the effect of Fe_3O_4 addition on the characterization of the formed Fe_3O_4/AC-ZnO nanocomposite and its impact on rhodamine B photodegradation.

Materials and Methods

Materials

Iron sand was used as the primary raw material. Sodium hydroxide (NaOH, analytical grade, Merck) and hydrochloric acid (HCl, 37 wt%, analytical grade, Merck) were employed for chemical activation and pH adjustment. Distilled water was used as the solvent in all experimental procedures. Coconut shell was utilized as the carbon precursor for material synthesis. Zinc nitrate tetrahydrate ($Zn(NO_3)_2{\cdot}4H_2O$, analytical grade, Merck) was used as the zinc source, while ethanol (C_2H_5OH, analytical grade, Merck) served as a dispersing and washing agent. Rhodamine B (analytical grade) was used as the model organic dye pollutant in the adsorption experiments.

Preparation of Fe_3O_4

The iron sand used was obtained from the Batanghari River, Jambi, located on Jl. Lintas Sumatera, Penyengat Rendah, Aur duri, Telanaipura District, Jambi City. Before being used for Fe_3O_4 synthesis, iron sand was obtained using a modified procedure carried out by [13]. Iron sand was washed and magnetized with a permanent magnet (20 g) dissolved in 37% HCl at 70˚C for as much as 53 ml. The solution formed was cooled and titrated with 12M NaOH at 70˚C for 48 ml until there was a precipitate. The precipitate that was successfully formed was then oven-dried at 1000˚C for 3 h. The resulting solid powder was characterized using VSM, XRF, and XRD.

Carbon Preparation and Activation

In this study, Carbon synthesis was carried out based on the synthesis procedure of the previous study [14]. A total of 500 g of coconut shell carbon was baked at 110˚C for 1 h, then mashed using a mortar and pestle. Coconut shell carbon was sieved with a 100-

mesh sieve to produce coconut shell carbon powder. Then, as much as 50 g of coconut shell carbon powder was put into a 500 mL beaker, and 250 mL of 1M NaOH solution was added. The solution was stirred using a magnetic stirrer for 4 h, accompanied by heating at 85˚C. The solution was filtered using filter paper and washed with distilled water until the pH was neutral (pH = 7). The residue was oven dried at 110˚C for 1 h. Then the dry powder was calcined at 600˚C for 1 h to obtain activated carbon.

Preparation of Fe_3O_4/AC.

The preparation of Fe_3O_4/AC uses a modified procedure carried out by Fini (2018) [15]. At the initial stage, magnetite was added with a ratio of (1,1), (2,1), (3,1) and (4,1) or as much as 0.25; 0.5; 0.75; 1 g respectively was dispersed into 100 ml of water and then 0.25 g activated carbon was added to the solution and the dispersion was transferred into a Teflon-coated stainless autoclave at 180˚C for 6 h. The precipitate was then washed with distilled water and ethanol. The results obtained were then characterized by XRD.

Synthesis of ZnO

In this study, the synthesis of ZnO was carried out based on the synthesis procedure of [14]. Zinc nitrate, 60 g of $Zn(NO_3)_2{\cdot}4H_2O$, was dissolved into 250 mL of distilled water and then stirred for 1 h at 80ºC at a constant speed. Then 1M NaOH solution was mixed dropwise into the solution until pH ~ 10 and stirred at 60ºC at a constant speed for 4 h, then allowed the solution to stand for 24 h at room temperature. Filtered and washed the precipitate using distilled water and ethanol until the pH was neutral. The precipitate was dried in an oven at 60ºC for 1 h and then calcined at 800ºC for 2 h. The solids obtained were then crushed and further characterized using FTIR, XRD, SEM-EDS, and a UV-Vis spectrophotometer.

Synthesis of Fe_3O_4/AC/ZnO

The synthesis of Fe_3O_4/AC/ZnO nanocomposite was carried out based on the modified procedure of [16], replacing rGO with AC because AC has the same structure as rGO. To prepare nanostructured Fe_3O_4/AC/ZnO, first, 500 mg of Fe_3O_4/AC and 500 mg of ZnO were dispersed separately in 60 mL of ethanol under ultrasonic treatment for 30 min. Then, the two solutions were mixed with vigorous stirring at 40 °C for 1 h. The results obtained were then collected with a permanent magnet and washed with distilled water. And than the Fe_3O_4/AC/ZnO obtained was dried under vacuum at room temperature overnight. In this study, the synthesis variables for Fe_3O_4/AC/ZnO were (0:1:1); (1:1:1); (2:1:1); (3:1:1); and (4:1:1). Finally, it was characterized using XRD, FTIR, VSM, and UV-Vis.

Rhodamine B photodegradation test using Fe_3O_4/AC/ZnO nanocomposite

50 ppm rhodamine B solution at neutral pH, and 200 mg of Fe_3O_4/AC/ZnO nanocomposite was added. The beaker was exposed to sunlight while stirring using a magnetic stirrer at a constant speed for 90 min. Then the suspension was filtered and the filtrate was measured for absorbance with a UV-Vis spectrophotometer at the maximum wavelength of rhodamine B.

Fe_3O_4/AC/ZnO nanocomposite characterization

Nanocomposite characterization was carried out using several instruments, such as crystal structure characterization using X-Ray Diffraction (XRD - X'Pert PRO Panalytical PW 30/40)), and compound composition analysis using X-ray Fluorescence (XRF - Panalytical Epsilon 3). Analysis of the

magnetic properties of nanocomposites using Vibrating Sample Magnetometer (VSM - OXFORD tipe 1,2H), surface morphological characteristics assessed by Scanning Electron Microscopy-Energy Dispersive Spectroscopy (SEM-EDS – Thermoscientific), and the photodegradation adsorbance of rhodamine B analyzed using UV-Vis Spectrophotometer (Halo DB 30).

Result and Discussions

XRF characterization

X-ray fluorescence (XRF) analysis was conducted to identify and quantify the elemental composition of iron sand collected from the Batanghari River, both before and after the magnetization process, as presented in Table 1. The results indicate that iron (Fe) is the dominant element, with a concentration of 74.1 wt.%, followed by silicon (Si) at 9.12 wt.% and titanium (Ti) at 7.82 wt.%. The high Fe content confirms that the iron sand is rich in iron-bearing minerals. The enrichment of Fe in the magnetic fraction can be attributed to the magnetic separation process, in which iron-containing minerals with strong magnetic or paramagnetic properties are preferentially attracted by the applied magnetic field. Consequently, the magnetization process effectively concentrates Fe within the iron sand, making it a suitable precursor for Fe_3O_4 synthesis in this study

Table 1. Elemental composition of iron sand determined by X-ray fluorescence (XRF) analysis.

Element	Value (%)
Al	3.18
Si	9.12
P	1.14
Ca	1.14
Ti	7.82
Fe	74.1
Ag	1.152

The Ti content was observed to increase after the magnetization process, which can be attributed to the magnetic behavior of Ti-containing minerals that are co-enriched during magnetic separation. This indicates that, in addition to iron, titanium-bearing phases are also concentrated in the magnetic fraction. Nevertheless, the high Fe content in the iron sand confirms its suitability as a reliable Fe source for Fe_3O_4 synthesis in this study.

XRD characterization (XRD)

characterization was conducted to identify the crystal structure, crystallinity, and crystal size. The sample analysis utilized XRD on an X-ray tube with Cu (λ = 1.54 Å), at a voltage of 40 kV and a current of 30.0 mA. Figure 1 is the result of XRD characterization of the synthesized Fe_3O_4 which is known to have 4 specific peaks with the highest intensity at 2θ angles at 30.23°; 35.60°; 57.11°; and 62.83°. Then the Fe_3O_4 peaks that appear show similarities with the peaks of Fe3O4 reference data JCPDS Number 01-075-0033 with positions 30.12 °; 35.48 °; 57.03 °; and 62.62 °. The same finding was reported by Researcher [13] the values for the peak of the angle 2θ at 30.09°; 35.42°; and 62.51°.

Figure 2 presents the XRD pattern of the activated carbon sample and its comparison with the standard reference data (JCPDS 00-025-0284). The diffractogram exhibits two broad diffraction features centered at 2θ ≈ 26.72° and 44.71°, corresponding to the

(002) and (100) crystallographic planes of carbon materials. The presence of these reflections, together with their broad and low-intensity profiles, indicates a predominantly amorphous carbon structure. The absence of sharp and well-defined diffraction peaks suggests a lack of long-range crystalline order, which is characteristic of activated carbon materials. The broadening of the (002) reflection further implies a disordered stacking of graphitic layers, commonly associated with high defect density and irregular carbon domains. Such amorphous characteristics are consistent with the reference JCPDS pattern and have been widely reported for activated carbons derived from biomass precursors.

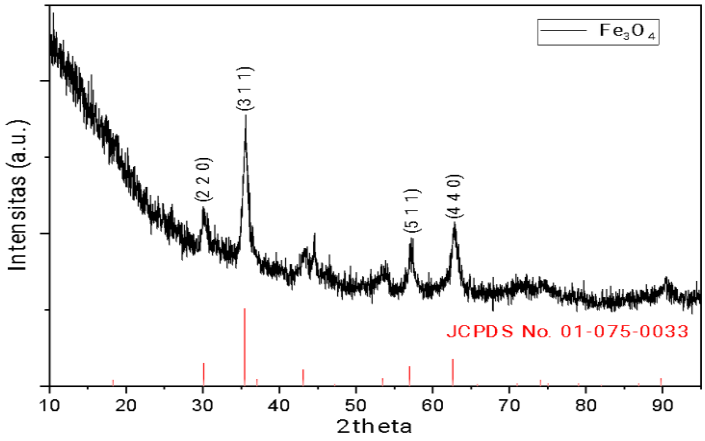

Figure 1. X-ray diffraction (XRD) pattern of the synthesized Fe_3O_4, showing characteristic diffraction peaks corresponding to the spinel crystal structure, in good agreement with the standard JCPDS card No. 01-075-0033.

The predominantly amorphous nature of the activated carbon is advantageous for adsorption and surface-mediated processes, as it is typically associated with high surface area and abundant active sites. These structural features are expected to contribute positively to the performance of the activated carbon when employed as a support material in the synthesized composite system.

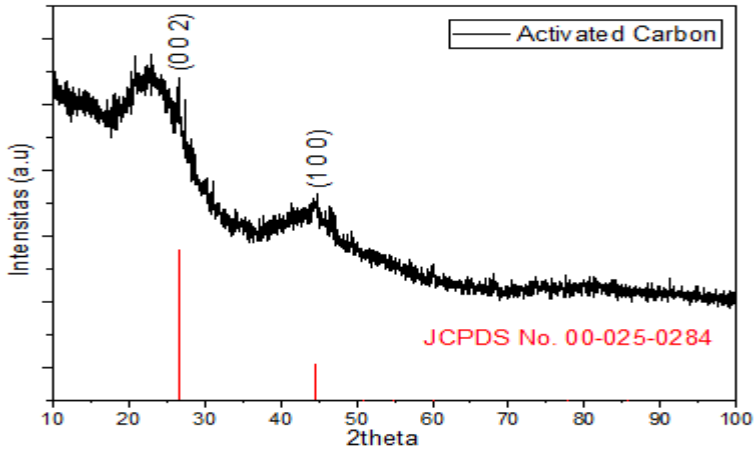

Figure 2. X-ray diffraction (XRD) pattern of the synthesized activated carbon, showing a broad diffraction peak characteristic of amorphous carbon structure, consistent with the standard JCPDS card No. 00-025-0284.

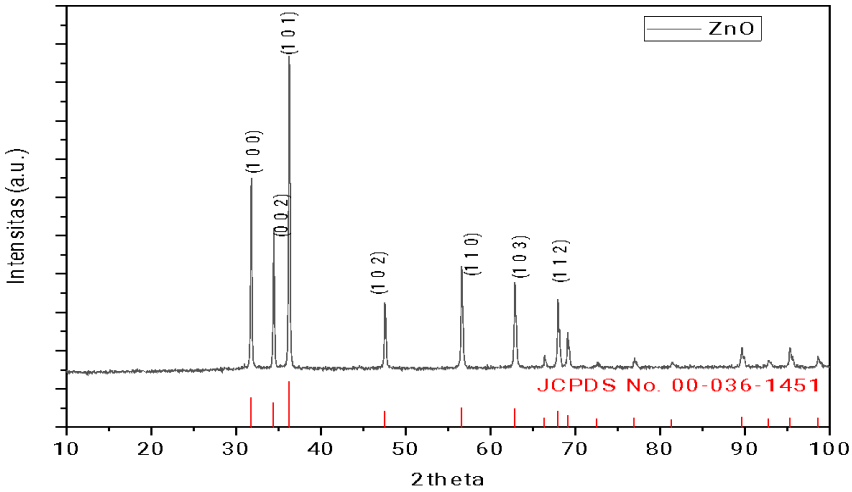

Figure 3. XRD diffractog of synthesized ZnO

Figure 3 shows the results of XRD characterization of ZnO. There are peak intensities located at 2θ angles with positions 31.82°; 34.47°; 36.30°; 47.59°; 56.63°; 62.89° and 67.98°. These results are close to JCPDS data No. 00-036-1451 and the research of [18] which showed diffraction peaks with high intensity at 2θ angles of 31.6°; 34.3°; 36.1°; 47.5°; 56.5°; 62.8°; and 67.9°.

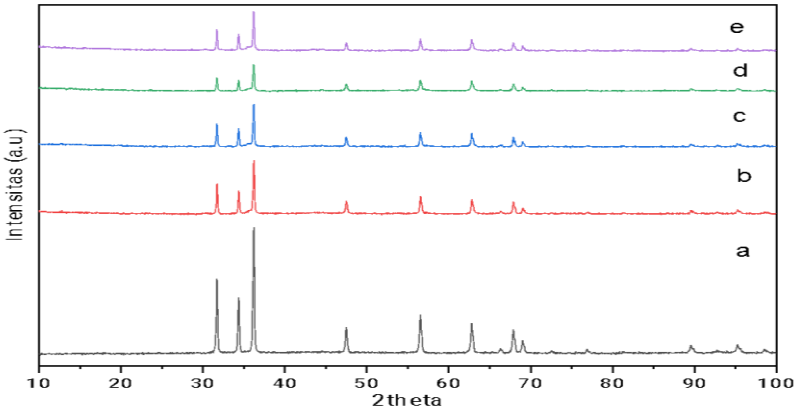

Figure 4. X-ray diffraction (XRD) patterns of Fe_3O_4/AC/ZnO nanocomposites with composition ratios: (a) 0:1:1, (b) 1:1:1, (c) 2:1:1, (d) 3:1:1, and (e) 4:1:1.

Table 2. Application of Strategies to Enhance the Bioavailability of Minerals

No	Sample	% Relative crystallinity	Crystal size (nm)
1	Fe_3O_4	-	23.97
2	ZnO	30.82	50.06
3	Fe_3O_4/AC/ZnO		
4	0:1:1	39.32	50.06
5	1:1:1	25.50	48.17
6	2:1:1	27.84	53.94
7	3:1:1	26.67	50.07
8	4:1:1	26.78	55.34

In Figure 4, the XRD characterization results of the Fe_3O_4/AC/ZnO nanocomposite show that ZnO peaks dominate the resulting diffractog peak pattern. However, the peaks that appear 2ɵ at 30.12°; 35.48°; 57.03°; and 62.62 indicate the formation of Fe3O4. Meanwhile, no peaks from AC were observed because AC has an amorphous phase. ZnO peaks were produced at 2ɵ at 31.82°; 34.47°; 36.30°; 47.59°; 56.63°; and 67.98. The resulting crystal structure shows that the combination of Fe3O4 and AC in ZnO does not trigger ion substitution in the ZnO lattice, so that the wurtzite structure of ZnO also does not experience changes [19].

The data in Table 2 show that The greater the mass of Fe_3O_4 added, the greater the crystal size of the resulting Fe_3O_4/AC/ZnO composite. Furthermore, synthesis conditions such as temperature and reaction time also influence crystal growth [20]. Fe_3O_4 acts as a nucleation site or template for the growth of ZnO on its surface. During the synthesis process, the interaction between the Fe_3O_4 surface and Zn^{2+} ions leads to the formation of ZnO around the Fe_3O_4. Consequently, the resulting ZnO crystals are generally larger than those formed from pure ZnO [21].

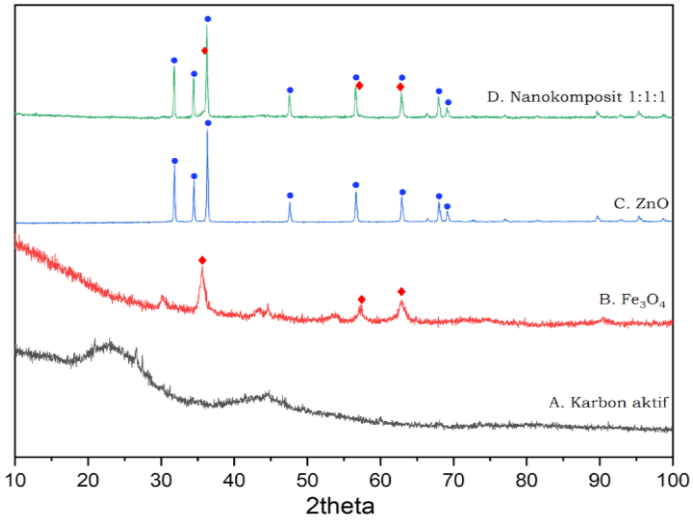

Figure 6. XRD diffractog (A) Activated carbon; (B) Fe_3O_4; C) ZnO; and (D) 1:1:1 Fe_3O_4 /AC/ZnO

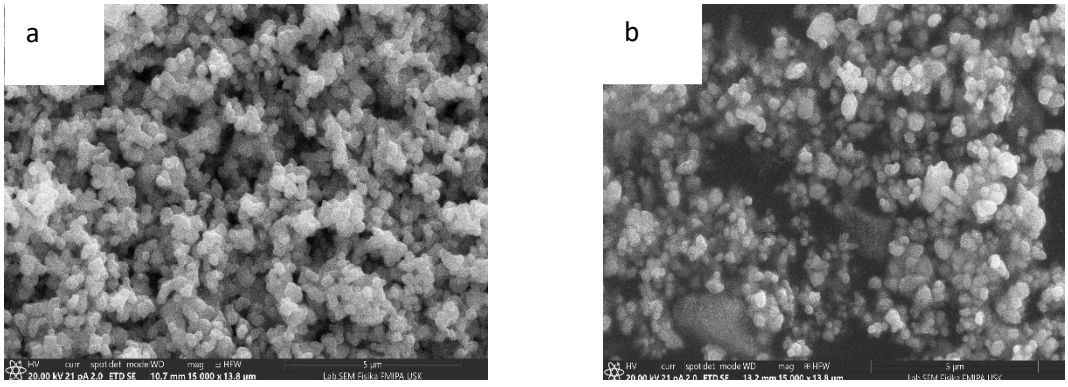

Figure 7. SEM a) ZnO and b) 1:1:1 Fe3O4/AC/ZnO nanocomposites synthesized

The Figure 6 shows that the intensity of activated carbon is nearly imperceptible, contributing only an amorphous phase to the 1:1 ratio nanocomposite. In the Fe3O4 diffractog, only a very weak intensity is observed at 2θ angle of 35.60°; 57.11°; and 62.83°.. In contrast, the intensity of ZnO is dominant, with peaks at the 2θ angles of

31.76°; 34.42°; 36.24°; 47.59°; 56.63°; 62.89° and 67.98°. These observed intensities indicate that the nanocomposite has been successfully synthesized.

Scanning Electron Microscopy (SEM)

To observe the morphological shape and distribution of particle dispersion, characterization was carried out using SEM. Morphological characterization of ZnO and 1:1:1 Fe3O4/AC/ZnO nanocomposite was carried out using SEM under the condition of voltage acceleration measurement of 20kV with 15000x magnification.

Figure 7 a is the SEM result of the ZnO nanocomposite, it is observed that the ZnO is irregularly round and spreads and accumulates between particles causing agglomeration on the entire surface while Figure 7 b shows the 1:1:1 Fe_3O_4/AC/ZnO nanocomposite formed showing that the ZnO particles stick and spread to the surface of the Fe_3O_4-AC which is cubic and hollow given by the activated carbon. It can be seen that there is still some Fe_3O_4 that has not been coated by activated carbon due to the lack of an impregnation process. It can be seen that the ZnO nanocomposite particles spread out, which results in a larger surface area, so that it can affect its photocatalytic activity. According to [22], the morphological shape of ZnO is round and fused. The particle size of ZnO and 1:1:1 Fe_3O_4/AC/ZnO nanocomposite was calculated using ImageJ standard software. It was found that ZnO nanoparticles and 1:1:1 Fe_3O_4/AC/ZnO nanocomposite had particle sizes of 57.95 nm and 42.74 nm, respectively. The particle size decreased in line with the crystal size, with a decrease in particle size being able to increase photocatalytic activity. According to [23], the smaller and more uniform particle size can increase photocatalytic activity due to the larger surface area.

Vibrating Sample Magnetometer (VSM)

To determine the magnetic strength of a sample, the VSM instrument also known as Vibrating Sample Magnetic is used. The following is the curve of Fe_3O_4 and 1:1:1 Fe_3O_4/AC/ZnO nanocomposite.

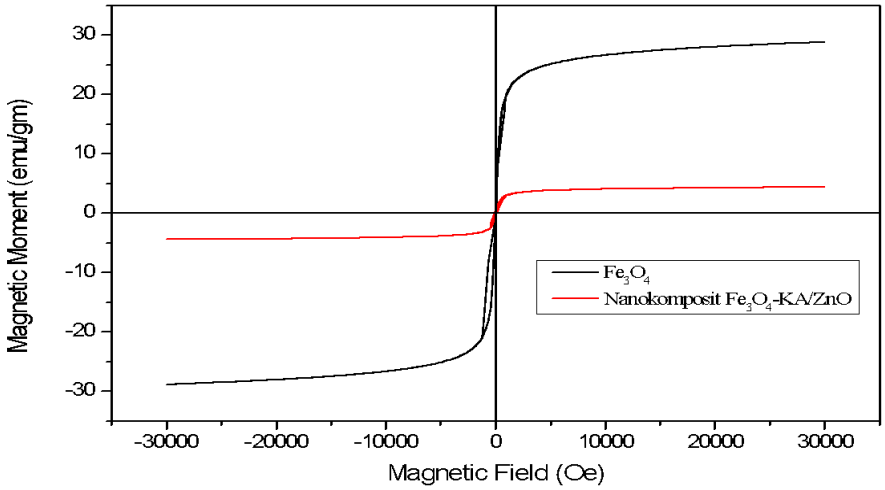

Figure 8. Hysteresis curve of Fe3O4 (A), 1:1:1 Fe_3O_4/AC/ZnO nanocomposite (B)

Table 3. VSM Characterization Result

Sample	Ms (emu/gr)
Fe_3O_4	28.8
1:1:1 Fe_3O_4/AC/ZnO nanocomposite	4.41

Figure 8 shows the hysterical curve of the nanocomposite synthesis results showing a decrease compared to Fe_3O_4. While in table 3 is the result of VSM characterization of Fe_3O_4 and 1:1:1 Fe_3O_4/AC/ZnO nanocomposite.

Table 3 shows that saturation magnetization (Ms) has decreased significantly with Fe3O4 of 28.8 emu/g with 1:1:1 Fe3O4/AC/ZnO nanocomposite of 4.41 emu/gr. With these results, it can be concluded that the magnetic strength the synthesis is superparamagnetic. Research conducted by [24] obtained a saturation magnetization of 25.7 emu/gr; these results are close to the results of the Fe3O4 synthesis that has been carried out. [25] obtained a saturation magnetization of 52.15 emu/gr, which was 2 times that of this study. According to [25], the smaller the crystal size, the smaller the number of magnetic domains, and the magnetic domain boundaries are also fewer, so that the saturation magnetization value (Ms) decreases. In nanocomposites, in addition to large crystal sizes, there are components that do not have magnetic or nonmagnetic properties, namely activated carbon, which can reduce the magnetic properties of the resulting nanocomposites. Research conducted by Astuti (2022) stated that the effect of adding carbon to the Fe3O4@ZnO-C nanocomposite was able to reduce the magnetic properties of the formed nanocomposite [26].

However, the superparamagnetic properties of the Fe3O4/AC/ZnO nanocomposite enable increased charge transfer and slow down the occurrence of electron-hole recombination, thereby enhancing photocatalytic activity and facilitating the separation process for reuse [27]. Photocatalytic Studies Photocatalyst tests were carried out with Fe3O4/AC/ZnO nanocomposite using parameters from the research of [10]. Performed in the time range 12.00-14.00 with an average luxmeter of 52350-53560, the photodegradation process was carried out with a concentration of rhodamine B of 50 ppm with a duration of sunlight irradiation for 90 min and was constantly stirred. The following is a data table of the % degradation of Rhodamine B used Fe3O4/AC/ZnO nanocomposites with various ratios.

Table 4. % Degradation of Rhodamine B with ratio of Fe_3O_4/AC/ZnO nanocomposite

Sample Name Fe_3O_4/AC/ZnO	Average Luxmeter	Average Initial Absorbance	Average final absorbance	Degradation of Rhodamine B (%)
0 : 1 : 1	53560	2.795	0.463	83.4
1 : 1 : 1	54670	2.795	0.109	96.1
2 : 1 : 1	52630	2.795	1.033	63.0
3 : 1 : 1	53123	2.795	0.479	82.8
4 : 1 :1	53340	2.795	0.712	74.5

Table 4 shows the percent degradation results from the photodegradation of Fe3O4/AC/ZnO nanocomposites, with the smallest percentage of 63% to 96.1%. It can be seen that the best percent degradation is in the nanocomposite with a ratio of 1:1:1, with a percent degradation of 96.1%. It can be seen that with the addition of Fe3O4, there is an increase from 83.4% to 96.1%. However, the 2:1:1 nanocomposite ratio experienced a significant decrease, then the 3,1 nanocomposite ratio increased, and the 4:1:1 nanocomposite decreased again. From the table, it can be seen that the higher the Fe3O4 ratio, the greater the decrease in absorbance percent is due to clumping that covers ZnO to carry out the photodegradation process. Because the greater

the ratio of Fe3O4, the percentage of rhodamine B absorbance decreases [28]. Nanocomposites with a ratio of 1:1:1 get the highest percent absorbance, which is comparable to the crystal size that has been characterized using XRD of 48.17nm. With the band gap energy obtained, the smaller the energy required for the degradation process. The smaller the band gap energy, the more OH● is formed and able to receive visible light. SEM results also show that ZnO is spread throughout the surface of Fe3O4/AC/ZnO, which causes more effectiveness in degrading rhodamine B substances.

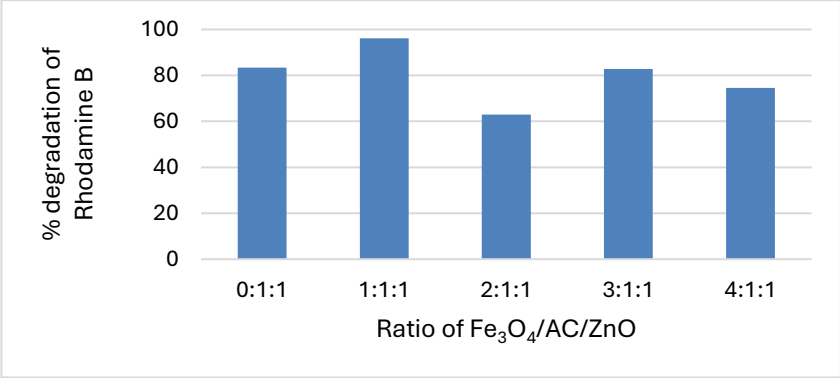

Figure 9. Graph of the relationship between the Fe_3O_4/AC/ZnO ratio and the % degradation of Rhodamine B

Where the smaller the crystal size and crystallinity, the greater the % absorbance obtained. Reducing crystal size and crystallinity enhances the % absorbance due to increased surface area, more defect states, and band gap narrowing. This can also be used for optimizing optical and photocatalytic properties [29].

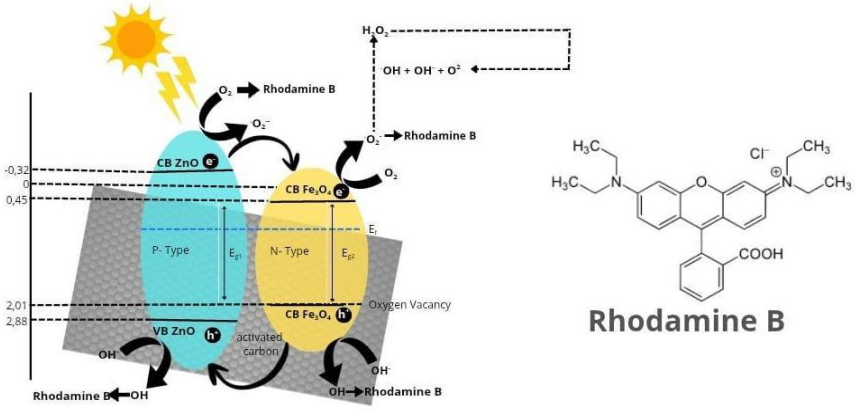

Figure 10. Photodegradation process of rhodamine B using Fe_3O_4/AC/ZnO nanocomposite

When the Fe_3O_4/AC/ZnO photocatalyst is exposed to photon energy from sunlight, Fe_3O_4 and ZnO will undergo a charge separation process that causes electron excitation from the valence band (VB) to the conduction band (CB) and produces holes in the VB. When forming the Fe_3O_4/AC/ZnO nanocomposite, Fe3O4 and ZnO are on the AC surface and can shift to longer wavelengths and produce smaller band gap energies, in accordance with the Z-scheme heterojunction of Fe_3O_4/AC/ZnO. The CB of ZnO is more positive than that of Fe_3O_4, but the VB of ZnO is more negative than that of Fe_3O_4 [30]. When exposed to photon energy from the sun, excited electrons from the CB

of ZnO will migrate to the VB of Fe3O4 [31]. Photogenerated electrons are captured by the AC surface through the semiconductor-heterojunction, preventing electron-hole recombination. Simultaneously, the same number of holes is formed in the semiconductor. The AC surface accepts electrons from the semiconductor CB, preventing electron recombination and significantly improving the photogenerated charge separation efficiency [32]. The separated holes and electrons will interact with O and OH– to produce reactive radical species •O2– and •OH. The radical species produced from the redox process then interact with Rhodamine B molecules, reducing the rhodamine B molecular chain into a simpler, environmentally friendly molecular chain [33].

Conclusion

Fe3O4/AC/ZnO nanocomposites have been successfully synthesized using the ultrasonic method. The addition of Fe3O4 variations affects the characteristics of the Fe3O4/AC/ZnO nanocomposites formed. The smallest crystal structure is produced from the 1:1:1 composition variation of the Fe3O4/AC/ZnO nanocomposite, specifically 48.17 nm, with a more dominant ZnO structure. Activated carbon does not affect the structure of the Fe3O4/AC/ZnO nanocomposite but affects the resulting magnetic properties. SEM results show that the 1:1:1 Fe3O4/AC/ZnO nanocomposite has a size of 42.74 nm with a more uniform surface morphology. The 1:1:1 Fe3O4/AC/ZnO nanocomposite exhibits superparamagnetic properties that facilitate increased charge transfer and slow down the occurrence of electron-hole recombination, thereby enhancing photocatalytic activity and reducing the need for separation for reuse. The 1:1:1 Fe3O4/AC/ZnO nanocomposite has the highest percentage of rhodamine B degradation, namely 96.1%. The magnitude of the ability of the Fe3O4/AC/ZnO nanocomposite to degrade rhodamine B will be developed by looking at the recycling ability of the Fe3O4/AC/ZnO nanocomposite for reuse in the rhodamine B photodegradation process

Acknowledgement

The authors would like to thank the University of Jambi for funding this research through the DIPA PNBP Science and Technology Applied Research Scheme with Research Contract Agreement Letter Number:369/UN21.11/PT.01.05/SPK/2023 Date 17 April 2023.

Author Contributions

Conceptualization, RB. and NP.; Methodology, PAW.; Software, R.; Validation, R., RB. and LA.; Formal Analysis, LM.; Investigation, LA. and PAW.; Resources, PAW.; Data Curation, RB.; Writing – Original Draft Preparation, RB. And PAW; Writing – Review & Editing, R. and LA.; Visualization, NP.; Supervision, LM.; Project Administration, RB.; Funding Acquisition, RB ; LM ; R ; NP".

Conflict of Interest

The authors declare no conflict of interest.

References

[1] Skjolding LM, Jørgensen LVG, Dyhr, KS, Köppl CJ, McKnight US, Bauer-Gottwein P, Mayer P, Bjerg PL, & Baun A. Assessing the Aquatic Toxicity and Environmental Safety of Tracer Compounds Rhodamine B and Rhodamine WT. *Water Research*. 2021; 197, 117109. https://doi.org/10.1016/j.watres.2021.117109

[2] Zilfa, Rahmayeni R, Setiadi Y, Adril A. Utilization of Natural Zeolite

Clinoptilolite-Ca as a Support of ZnO Catalyst for Congo-red Degradation and Congo-red Waste Applications with Photolysis. *Oriental Journal of Chemistry*. 2018; 34(2), 887-893. https://doi.org/10.13005/ojc/340237

[3] Das PP, Sharma M, Purkait MK. Recent progress on electrocoagulation process for wastewater treatment: A review. *Separation and Purification Technology*. 2022; 292:121058. https://doi.org/10.1016/j.seppur.2022.121058

[4] Silva LRd, Araujo TJR, Fonseca MTS, Santos NC, Gomes GE, Gomes JP, Araujo GT, Rocha APT. Application of Photo-Fenton Oxidative Process Followed by Adsorption in Dairy Effluents Treatment. Journal of Water Process Engineering. 2024; 68: 106365. https://doi.org/10.1016/j.jwpe.2024.106365

[5] Priya ES, Selvan PS. Water Hyacinth (Eichhornia Crassipes) – An Efficient and Economic Adsorbent for Textile Effluent Treatment – A Review. *Arabian Journal of Chemistry*. 2017; 10(2), 1-11. http://dx.doi.org/10.1016/j.arabjc.2014.03.002

[6] Tashakkori Masuleh MT, Hasheminiasari M, Ashiri R. Enhanced Photocatalytic Efficiency of Eco-Friendly Synthesized ZnO for Rapid Full Degradation of Methylene Blue Dye. *Materials Advances*. 2025; 2611–2621. https://doi.org/10.1039/d5ma00026b

[7] Raha S, Ahmaruzzaman M. ZnO nanostructured materials and their potential applications: progress, challenges and perspectives. *Nanoscale Advances*. 2022; *4*(8), 1868–1925. https://doi.org/10.1039/d1na00880c

[8] Rungsawang T, Krobthong S, Paengpan K, Kaewtrakulchai N, Manatura K, Eiad-Ua A, Boonruang C, Wongrerkdee S. Synergy of Functionalized Activated Carbon and ZnO Nanoparticles for Enhancing Photocatalytic Degradation of Methylene Blue and Carbaryl. *Radiation Physics and Chemistry*. 2024; 223 : 111924 https://doi.org/10.1016/j.radphyschem.2024.111924

[9] Khalid A, Ahmed RM, Taha M, Soliman TS. Fe_3O_4 nanoparticles and Fe_3O_4 @SiO_2 core-shell: synthesize, structural, morphological, linear, and nonlinear optical properties. *Journal of Alloys and Compounds*. 2023; *947*, 169639. https://doi.org/10.1016/j.jallcom.2023.169639

[10] Saflou M, Allahyari S, Rahemi N, Tasbihi, M. Oil Spill Degradation Using Floating Magnetic Simulated Solar Light-Driven Nano Photocatalysts Of Fe_3O_4-ZnO Supported On Lightweight Minerals. *Journal of Environmental Chemical Engineering*. 2021; *9*(4) : 105268. https://doi.org/10.1016/j.jece.2021.105268

[11] Rini NP, Zurnansyah, Larasati DA, Mahardhika LJ, Jayanti PD, Kusumah HP, Istiqomah NI, Tumbelaka RM, Asri NS, Angel J, Kato T, Oshima D, Aliah H, Kusumaatmaja A, Suharyadi E. Photocatalytic Degradation of Rhodamine B Using A Reusable and Magnetically Separable Fe_3O_4/rGO/ZnO Nanocomposite Synthesized Through Green Approach Utilizing Plant Leaf Extracts. *Journal of Science: Advanced Materials and Devices*. 2024;*9*(4) : 100812. https://doi.org/10.1016/j.jsamd.2024.100812

[12] Wang Y, Gao J, Liu Y, Li M, Zhang M, He G, Sun Z. Facile Fabrication of ZnO Nanorods Modified Fe_3O_4 Nanoparticles with Enhanced Magnetic, Photoelectrochemical and

Photocatalytic Properties. *Optical Materials.* 2021;111 : 110608. https://doi.org/10.1016/j.optmat.2020.110608

[13] Hefdea A, Rohmawati L Sintesis Fe_3O_4 dari Pasir Mineral Tulungagung Menggunakan Metode Kopresipitasi.. *Inovasi Fisika Indonesia*. 2020; 9(2), 1-4. https://doi.org/10.26740/ifi.v9n2.p1-4

[14] Bemis R, Nelson, Ngatijo, Nurjanah S, Maghviroh N. Sintesis dan karakterisasi fotokatalis ZnO/karbon aktif dan aplikasinya pada degradasi rhodamin B. *Chempublish Journal*. 2019: 4(2), 101–113. https://doi.org/10.22437/chp.v4i2.7936

[15] Kimiagar S, Mirazimi H. Hydrothermal Synthesis of Fe_3O_4-ZnO Nanocomposites for Removing Fluoride from Water. *Progress in Physics of Applied Materials*. 2024; *4*(1), 63–69. https://doi.org/10.22075/ppam.2024.33571.1092

[16] Abharya A, Gholizadeh A. Synthesis of a Fe_3O4-rGO-ZnO Catalyzed Photo-Fenton System with Enhanced Photocatalytic Performance. *Ceramics International*. 2021; Vol. 47(9) :12010-12019. https://doi.org/10.1016/j.ceramint.2021.01.044

[17] Shamsuddin MS, Yusoff NRN, Sulaiman MA. Synthesis and Characterization of Activated Carbon Produced from Kenaf Core Fiber Using H_3PO_4 Activation. *Procedia Chemistry*. 2016; 16(1), 558-565. https://doi.org/10.1016/j.proche.2016.03.053

[18] Hernowo A, Nurhasanah I. Kristalinitas dan Ukuran Nanopartikel ZnO yang dikalsinasi pada Temperatur 100^{o}C dan 200^{o}C. *Jurnal Fisika Teori, Eksperimen dan Fisika Aplikasi*. 2019, 22(4), 123-131

[19] Salem BB, Essalah G, Ameur SB, Duponchel B, Guermazi H, Guermazi S, Leroy G. Synthesis and Comparative Study of the Structural and Optical Properties of Binary ZnO-Based Composites for Environmental Applications. *Royal Society of Chemistry*. 2023; 13, 6287. https://doi.org/10.1039/d2ra07837f

[20] Hoai LP, Van DN, Van KN, Thi HPP. Rational Design of Magnetically Separable Core/Shell Fe_3O_4/ZnO Heterostructures for Enhanced Visible-Light Photodegradation Performance. *Royal Society Of Chemistry*. 2021; 11, 22317. https://doi.org/10.1039/d1ra03468e

[21] Poonam D, Dwivedi, Indu J, Azhar UK, Azmat AK. Photoremediation of Methylene Blue by Biosynthesized ZnO/Fe_3O_4 Nanocomposites Using *Callistemon Viminalis* Leaves Aqueous Extract: A Comparative Study. *Nanotechnology Reviews*. 2021; 1912–1925. https://doi.org/10.1515/ntrev-2021-0117

[22] He R, Xu, Cheng B, Yu J, Ho W. Review on Nanoscale Bi-based Photocatalysts. *Nanoscale Horizons*. 2018; 3(3), 464. https://doi.org/10.1039/C8NH00062J

[23] Swastika PE, Hardheyanti F, Prasetyowati R, Ariswan A, Warsono W. Pengaruh Konsentrasi HCl terhadap Mikrostruktur dan Sifat Kemagnetan Nanopartikel Fe_3O_4 yang Disintesis dari Pasir Besi Pantai Glagah Kulonprogo. *Jurnal Sains Dasar*. 2021; 10(1), 24-29. https://doi.org/10.21831/jsd.v10i1.39141

[24] Simamora P, Krisna K. Sintesis dan Karakterisasi Sifat Magnetik Nanokomposit Fe_3O_4-Montmorilonit Berdasarkan Variasi Suhu. *Prosiding Seminar Nasional Fisika*. 2015; 75-80.

[25] Siagian SM, Khairani S, Chrsina S, Tampubolon FR. Sintesis dan

Karakteristik Sifat Optik Semikonduktor ZnO dan ZnO Dopping Cu. *Jurnal Pendidikan dan Ilmu Fisika*. 2022; 8(1), 79-83.

[26] Astuti A, Arief S, Pebrina D. Effect of the Amount of Carbon in the Fe_3O_4@ZnO-C Nanocomposites on Its Structure and Magnetic Properties. *Jurnal Kimia Sains dan Aplikasi*. 2022; 362-367. https://doi.org/10.14710/jksa.25.10.362-367

[27] Raha S, Ahmaruzzaman M. Enhanced Performance of a Novel Superparamagnetic G-C_3N_4 /NiO/ZnO/Fe_3O_4 Nanohybrid Photocatalyst for Removal of Esomeprazole: Effects of Reaction Parameters, Co-Existing Substances and Water Matrices. *Chemical Engineering Journal*. 2020. 395 (2020) 124969. https://doi.org/10.1016/j.cej.2020.124969

[28] Suprihatin IE, Murdani ND, Suarsa IW. Bentonit-Fe_3O_4 Sebagai Fotokatalis Dalam Proses Fotodegradasi Naphthol Blue Black Dengan Iradiasi Uv. *Jurnal Kimia*. 2021; 15(1), 59-66. https://doi.org/10.24843/JCHEM.2021.v15.i01.p09

[29] Jessica M, Asuka N, Fangda J, Marie Y, and Shin-ichi O. The Absorption Properties of ZrO_2 Nanoparticles in the THz and sub-THz Frequency Ranges. *Royal Society of Chemistry*. 2024; 14, 7903–7909 | 7903. https://doi.org/10.1039/d3ra07970h

[30] Yang H, Wei C, Hongfei L, Minshen Z, Fuwei L, Qi X, Zengxia P, Zifeng W, Lei W, Yan H, Chunyi Z. Graphene Stirrer with Designed Movements: Targeting on Environmental Remediation and Supercapacitor Applications. *Green Energy & Environment*. 2018; 86-96. https://doi.org/10.1016/j.gee.2017.10.004

[31] Pham TLH, Nguyen VQ, Nguyen TH, Ha TH, Duong AT, Manh TT, Quang VT, Ta NB, Nguyen T, Van-Duong D. Efficiency Enhancement of Photocatalytic Activity under UV and Visible Light Irradiation using ZnO/Fe_3O_4 Heteronanostructures. *Solar Energy*. 2023; 712-724. https://doi.org/10.1016/j.solener.2022.12.011

[32] Hasniah A, Nugraheni PR, Irfan SF, Zurnansyah Z, Larrisa JM, Putri DJ, Hafil PK, Rivaldo MT, Nurul II, Nining SA, Ryan NI, Edi S. Microstructures, Optical, Magnetic Properties, and Photocatalytic Activity of Magnetically Separable and Reusable ZnO-Doped Fe_3O_4/rGO Nanocomposite Synthesized Via Green Route. *Carbon Resources Conversion*. 2024; 100235. https://doi.org/10.1016/j.crcon.2024.100235

[33] Nugraheni PR, Zurnansyah Z, Dyah AL, Larrisa JM, Putri DJ, Hafil PK, Nurul II, Rivaldo MT, Nining S., Julia A, Takeshi K, Daiki O, Hasniah A, Ahmad K, Edi S. Photocatalytic degradation of Rhodamine B using a Reusable and Magnetically Separable Fe_3O_4/rGO/ZnO Nanocomposite Synthesized through Green Approach Utilizing Plant Leaf Extracts. *Journal of Science: Advanced Materials and Devices*. 2024, 100812. https://doi.org/10.1016/j.jsamd.2024.100812